

# Gradual Changes in the Aromaticity in a Series of Hydroxypyridine-Carboxylic Acid Derivatives and Their Effect on Tautomerism and Crystal Packing

Published as part of *Crystal Growth & Design* virtual special issue “Legacy and Future Impact of the Cambridge Structural Database: A Tribute to Olga Kennard”.

Nóra V. May,\* G. Tamás Gál, Tamás Holczbauer, Laura Bereczki, Valerio B. Di Marco, and Petra Bombicz



Cite This: *Cryst. Growth Des.* 2024, 24, 1096–1109



Read Online

ACCESS |



Metrics & More

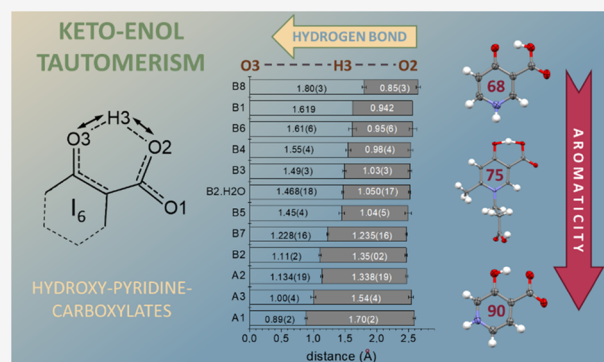


Article Recommendations



Supporting Information

**ABSTRACT:** The keto–enol tautomerism of hydroxypyridine-carboxylic acid (HPC) derivatives with proton transfer between the hydroxyl or carboxyl oxygen atoms was investigated in the case of three 3-hydroxy-4-pyridine-carboxylic acid (3HPC) and eight 4-hydroxy-3-pyridine-carboxylic acid (4HPC) derivatives containing altered pyridine ring substituents. Due to the vicinal position of hydroxyl and carboxylate groups, the hydroxyl proton is involved in an intramolecular H-bond and can very easily transform into the keto or enol tautomer. The proton position was found to correlate with the aromaticity of the pyridine ring, which was described by the Bird index, calculated on the basis of the measured atomic distances. Due to the planar shape of the molecules,  $\pi\cdots\pi$  stacking and/or C–O $\cdots\pi$  interactions were found in all investigated compounds. The molecular properties along with their main supramolecular interactions were compared. Packing arrangements and the main hydrogen-bonding schemes were further compared by using Hirshfeld surface analysis. In the case of the four *N*-methyl-substituted 4HPC derivatives, the synthon consisting of hydrogen bonds was preserved in the plane of the molecules despite the presence of the various ring substituents. Pairing the 3HPC and 4HPC derivatives, the corresponding compounds exhibited the same molecular shape but different nitrogen positions in the pyridine ring. This gave us the opportunity to examine how the difference in the electron distribution affects only and exclusively the secondary interactions and the arrangement of the molecules in the crystals. The electrostatic potential was calculated and mapped over the Hirshfeld surface, and the calculations of pairwise interaction energies and total energy frameworks were performed using the B3LYP/6-31G(d,p) energy model.



## INTRODUCTION

The tautomers are interconvertible organic compounds that differ only in the positions of the protons and electrons. Prototropy, the keto–enol tautomerism, is a commonly occurring process. The migration of a hydrogen atom is accompanied by the alteration of the electron density distribution of the substituted ring. The Cambridge Structural Database as a whole is also a collection of tautomeric forms of compounds. Although CSD version 2023.02.0 gives 262 hits searching for the word “tautomer”, there may certainly be many more nonflagged cases. The tautomeric pairs represent the two extremes: the keto and the enol forms. Thereby, we report a family of hydroxypyridine-carboxylic acid derivatives, where a gradual change of aromaticity is induced due to ring substituents of different positions and properties. The gradual alteration of aromaticity results in the fine-tuning of the position of the keto/enol O $\cdots$ H $\cdots$ O proton in the investigated compounds. It

provides us the opportunity to study the relationship between aromaticity and tautomerism as well as their effect on crystal packing.

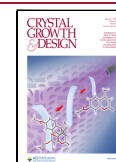
Aromatic compounds play key roles in the biochemistry of all living organisms, as aromatic groups can be found in several amino acids and nucleotides. Aromaticity is a property that gives increased stability and lower reactivity compared to saturated compounds having single bonds. In the heterocyclic aromatic ring pyridine, the presence of a nitrogen atom in the aromatic

**Received:** September 21, 2023

**Revised:** December 15, 2023

**Accepted:** December 15, 2023

**Published:** January 10, 2024



ring reduces the aromaticity of the ring and thereby increases its reactivity. Experimental investigation of aromaticity is not easy in such a delocalized electron system, but X-ray diffraction provides this opportunity because it is able to measure the distance of nonhydrogen atoms with high precision. When the pyridine ring contains a hydroxyl and carboxyl group in the vicinal position, like in 3- or 4-hydroxypyridine-carboxylic acid (HPC) derivatives, an intramolecular hydrogen bond can form in their neutral (zwitterionic) form between the two functional groups. Consequently, HPC derivatives can very easily transform into the keto or enol tautomer, giving the well-known phenomenon, the keto–enol tautomerism<sup>1</sup> (Figure S1).

In this work, we present the results of crystallization, single-crystal determination, and systematic structural comparison of three 3-hydroxy-4-carboxylate (3HPC, A1–A3) and seven 4-hydroxy-3-carboxylate (4HPC, B2–B8) derivatives together with the extreme of the B series, Form I polymorph of B1 (first determined by Santos et al.,<sup>2</sup> CSD refcode KUXPUP), as comparison. Figure 1 shows the diagram of the formulas of the

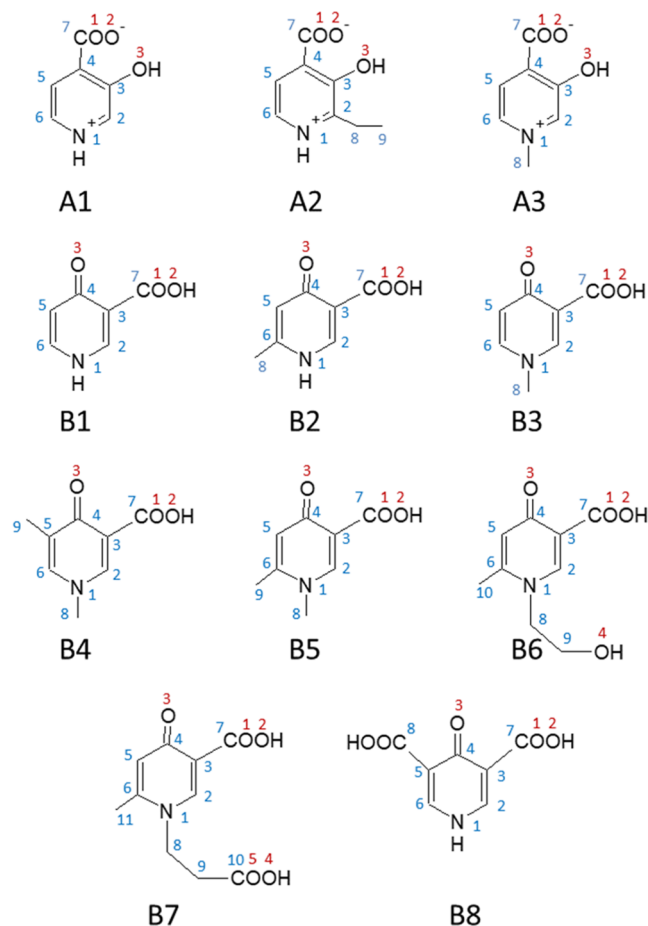


**Figure 1.** Diagram of the formulas of the investigated compounds in their enol (A1–A3) and keto (B1–B8) forms with atom numbering.

investigated compounds: 3-hydroxypyridinium-4-carboxylate (A1), 2-ethyl-3-hydroxypyridinium-4-carboxylate (A2), 1-methyl-3-hydroxypyridinium-4-carboxylate (A3), 4-oxo-1,4-dihydropyridine-3-carboxylic acid (B1), 6-methyl-4-oxo-1,4-dihydropyridine-3-carboxylic acid (B2), 1-methyl-4-oxo-1,4-dihydropyridine-3-carboxylic acid (B3), 1,5-dimethyl-4-oxo-1,4-dihydropyridine-3-carboxylic acid (B4), 1,6-dimethyl-4-oxo-1,4-dihydropyridine-3-carboxylic acid (B5), 1-(2-hydrox-

yethyl)-6-methyl-4-oxo-1,4-dihydropyridine-3-carboxylic acid (B6), 1-(2-carboxyethyl)-6-methyl-4-oxo-1,4-dihydropyridine-3-carboxylic acid (B7), and 4-oxo-1,4-dihydropyridine-3,5-dicarboxylic acid (B8).

The keto–enol tautomerism of 4-hydroxy-3-pyridine-carboxylic acid (B1), aka 4-hydroxy-nicotinic acid, was studied in detail in the solid phase by Long et al.,<sup>3</sup> where both tautomers could be detected in different crystal forms. Three anhydrides and two hydrates of B1 were crystallized and measured by the single crystal X-ray diffraction (SC-XRD) technique. In the Form I (CSD refcode KUXPUP02) and Form II (CSD refcode KUXPUP01) crystals, the molecules were found in the keto form, while in Form III (CSD refcode AKIHAF), the enol form exists. A hemihydrate was found in the keto form (CSD refcode AVEMUK) and a monohydrate in the enol form (CSD refcode AKIHIN) of B1 (Figure S1). It was recognized that the direction of the N–H group of the neighboring pyridine toward the OH and COO<sup>−</sup> groups influenced the position of the proton in the intramolecular hydrogen bond. The molecule prefers to crystallize in the keto form in a polarized environment, but the enol form can form stronger intermolecular hydrogen bonds with the deprotonated carboxylate group.

HPC derivatives have been proposed recently as potential chelating agents for Fe(III) and Al(III) to overcome the side effects of deferiprone (3-hydroxy-1,2-dimethylpyridin-4(1H)-on), a widely used chelator. Their favorable properties include low toxicity, no redox activity, and high complex stability.<sup>4,5</sup> The effect of aromaticity on the proton dissociation process is important because this proton is replaced by the metal ion during chelation therapy. In our previous studies, we investigated the complexation properties of selected 3HPC and 4HPC derivatives with copper(II)<sup>6</sup> and with zinc(II).<sup>7</sup> The bis-ligand complexes with [O<sup>−</sup>,O<sub>carb</sub><sup>−</sup>][O<sup>−</sup>,O<sub>carb</sub><sup>−</sup>] equatorial coordination crystallized in all cases, but the electron distribution in the ligand influences the type of the axial coordination of the metal center in dimeric complexes. Hydroxyl oxygen coordinates in 3HPC derivatives and the carboxylate oxygen coordinates in 4HPC derivatives axially. The acidity of the hydroxyl group also affects the strength of the complex formation, as a positive correlation has been found between the acidity of the OH group and the complex formation ability of the ligands with copper(II).<sup>6</sup>

In this work, our goal was to investigate three 3-hydroxy-4-pyridine-carboxylic acid (3HPC) and eight 4-hydroxy-3-pyridine-carboxylic acid (4HPC) derivatives with varying proton donor and acceptor substituents regarding their aromaticity and study their effect on keto–enol tautomerism. The electrostatic and steric effects of the substituents have been investigated on the tautomeric molecular structures and crystal packing arrangements. The partial or complete elimination of the aromaticity of the pyridine ring is expected when the keto tautomer is formed. The position of the proton involved in an intramolecular interaction between the hydroxyl and carboxylate oxygen atoms, along with the heavy atom distances, informs us about the electron distribution on the oxygen donor atoms and the aromaticity of the pyridine ring.

A complex structural analysis was performed to reveal the steric and electronic effects of the different donor groups on the aromaticity of the pyridine ring and the packing arrangements of the molecules. The strong and weak intermolecular interactions (O/N–H...O/S/N, C–H...O, C/O–H... $\pi$ ,  $\pi$ ... $\pi$ , etc.) were investigated using Hirshfeld surface analysis. Additionally, interaction energy and total energy frameworks were calculated

**Table 1. Crystal Data and Structure Refinement Parameters of Crystals A1, A2, A3, B1, B2, and B2·H<sub>2</sub>O**

	A1	A2	A3	B1 <sup>a</sup>	B2	B2·H <sub>2</sub> O
CCDC number	1951148	1951149	1951150	768692	1951151	1951152
formula	C <sub>6</sub> H <sub>5</sub> NO <sub>3</sub>	C <sub>8</sub> H <sub>9</sub> NO <sub>3</sub>	C <sub>7</sub> H <sub>7</sub> NO <sub>3</sub>	C <sub>6</sub> H <sub>5</sub> O <sub>3</sub> N	C <sub>7</sub> H <sub>7</sub> NO <sub>3</sub>	C <sub>7</sub> H <sub>9</sub> NO <sub>4</sub>
formula weight	139.11	167.16	153.14	139.11	153.14	171.15
color/shape	yellow/prism	colorless/prism	colorless/block		colorless/platelet	colorless/prism
crystal size (mm)	0.25 × 0.25 × 0.25	0.25 × 0.15 × 0.10	0.50 × 0.18 × 0.15		0.50 × 0.50 × 0.05	0.50 × 0.10 × 0.10
T/K	293(2)	103(2)	93(2)	293(2)	103(2)	103(2)
crystal system	monoclinic	orthorhombic	monoclinic	monoclinic	monoclinic	monoclinic
space group	<i>P</i> 2 <sub>1</sub> / <i>n</i>	<i>Pbca</i>	<i>P</i> 2 <sub>1</sub> / <i>c</i>	<i>P</i> 2 <sub>1</sub> / <i>c</i>	<i>P</i> 2 <sub>1</sub> / <i>n</i>	<i>P</i> 2 <sub>1</sub> / <i>c</i>
<i>a</i> (Å)	5.4668(3)	7.5221(4)	4.9126(4)	3.804(3)	4.7412(5)	3.7841(3)
<i>b</i> (Å)	5.1126(4)	7.3103(4)	11.9096(7)	14.582(7)	11.3249(14)	16.3965(16)
<i>c</i> (Å)	20.5591(15)	27.8062(19)	11.1748(6)	10.673(6)	13.1688(16)	12.3984(13)
β (deg)	95.303(2)	90	92.244(5)	94.254	98.262(4)	93.635(3)
volume (Å <sup>3</sup> )	572.16(7)	1529.03(16)	653.30(7)	590.4(6)	699.74(14)	767.72(13)
Z/Z'	4/1	8/1	4/1	4/1	4/1	4/1
λ (Å)						
<i>D</i> <sub>calc</sub> (Mg/m <sup>3</sup> )	1.615	1.452	1.557	1.565	1.454	1.481
abs. coeff., μ (mm <sup>−1</sup> )	0.132	0.112	1.052	1.103	0.115	0.123
<i>F</i> (000)	288	704	320	288	320	360
θ range (deg)	3.783–26.361	3.079–27.462	7.438–71.653	5.14–66.95	3.126–27.464	3.293–27.463
completeness to 2θ	0.999	0.999	0.869	0.949	0.999	0.998
data/restraints/param.	1173/0/94	1746/0/113	1072/0/104	999/0/112	1593/0/104	1742/0/119
goodness of fit on <i>F</i> <sup>2</sup>	1.122	1.130	1.125	1.034	1.006	1.125
<i>R</i> <sub>1</sub> , <i>wR</i> <sub>2</sub> [ <i>I</i> > 2σ( <i>I</i> )]	0.0457, 0.1260	0.0674, 0.1463	0.0399, 0.0992	0.0364	0.0556, 0.1234	0.0406, 0.1036
<i>R</i> <sub>1</sub> , <i>wR</i> <sub>2</sub> (all data)	0.0521, 0.1339	0.0887, 0.1649	0.0436, 0.1028	0.0476	0.0792, 0.1360	0.0484, 0.1078

<sup>a</sup>Data taken from ref 2 (CSD refcode KUXPUP).

**Table 2. Crystal Data and Structure Refinement Parameters of Crystals B3–B8**

	B3	B4	B5	B6	B7	B8
CCDC number	1951153	1951154	1951155	1951156	1951157	1951158
formula	C <sub>7</sub> H <sub>7</sub> NO <sub>3</sub>	C <sub>8</sub> H <sub>9</sub> NO <sub>3</sub>	C <sub>8</sub> H <sub>9</sub> NO <sub>3</sub>	C <sub>9</sub> H <sub>11</sub> NO <sub>4</sub>	C <sub>10</sub> H <sub>11</sub> NO <sub>5</sub>	C <sub>7</sub> H <sub>9</sub> NO <sub>5</sub>
formula weight	153.14	167.16	167.16	197.19	225.20	183.12
color/shape	colorless/platelet	colorless/platelet	colorless/prism	colorless/platelet	colorless/chunk	colorless/prism
crystal size (mm)	0.50 × 0.20 × 0.05	0.50 × 0.30 × 0.05	0.30 × 0.20 × 0.10	0.30 × 0.25 × 0.05	0.50 × 0.50 × 0.30	0.10 × 0.10 × 0.05
T/K	293(2)	103(2)	103(2)	103(2)	103(2)	103(2)
crystal system	monoclinic	orthorhombic	orthorhombic	orthorhombic	monoclinic	monoclinic
space group	<i>Cc</i>	<i>Pca</i> 2 <sub>1</sub>	<i>Pccn</i>	<i>Pna</i> 2 <sub>1</sub>	<i>P</i> 2 <sub>1</sub> / <i>c</i>	<i>P</i> 2 <sub>1</sub> / <i>n</i>
<i>a</i> (Å)	3.8931(12)	13.796(2)	7.6997(3)	6.7714(6)	10.9193(11)	6.7557(6)
<i>b</i> (Å)	15.733(3)	7.2871(11)	10.8856(4)	15.8849(15)	8.2883(8)	11.6191(11)
<i>c</i> (Å)	11.238(4)	7.4025(10)	17.6722(6)	8.2486(6)	11.1679(11)	9.2953(10)
β (deg)	94.599(7)	90	90	90	109.663(3)	105.809(3)
volume (Å <sup>3</sup> )	686.1(3)	744.21(19)	1481.21(9)	887.24(13)	951.78(16)	702.04(12)
Z/Z'	4/1	4/1	8/1	4/1	4/1	4/1
λ (Å)						
<i>D</i> <sub>calc</sub> (Mg/m <sup>3</sup> )	1.483	1.492	1.499	1.476	1.572	1.733
abs. coeff., μ (mm <sup>−1</sup> )	0.118	0.115	0.978	0.117	0.128	0.151
<i>F</i> (000)	320	352	704	416	472	376
θ range (deg)	3.164–27.480	3.162–25.327	5.005–68.230	3.270–27.478	3.129–27.469	3.335–27.478°
completeness to 2θ	0.998	0.997	1.000	0.995	0.999	0.999
data/restraints/param.	1553/0/104	1353/0/114	1360/0/114	1973/1/134	2180/0/152	1610/0/124
goodness of fit on <i>F</i> <sup>2</sup>	1.098	1.042	1.135	1.043	1.103	1.076
<i>R</i> <sub>1</sub> , <i>wR</i> <sub>2</sub> [ <i>I</i> > 2σ( <i>I</i> )]	0.0464, 0.1055	0.0559, 0.1445	0.0350, 0.0854	0.0594, 0.1451	0.0385, 0.0988	0.0610, 0.1231
<i>R</i> <sub>1</sub> , <i>wR</i> <sub>2</sub> (all data)	0.0545, 0.1100	0.0594, 0.1483	0.0365, 0.0864	0.0808, 0.1620	0.0405, 0.1005	0.0826, 0.1313

to compare the strength and nature of noncovalent interactions for the selected group of compounds. The understanding of the effect of the various substituents on the electron distribution of the main donor groups (hydroxyl and carboxyl) and on the aromaticity of the pyridine ring in HPC molecules may support their development as potential chelator ligands.

## EXPERIMENTAL SECTION

**Crystal Growth.** Hydroxypyridinecarboxylic acid derivatives were received from the University of Padova. The compounds were synthesized as described previously.<sup>6,8–10</sup> The compounds were used without further purification. In the previous papers,<sup>4,5</sup> compounds

A1–A3 were named 3H4P (or DT0), DT21, and DT1, whereas compounds B1–B8 were named 4H3P (or DQ0), DQ6, DQ1, DQ715, DQ716, DQ7176, DQ7165, and DQ58, respectively. Single crystals



suitable for X-ray diffraction analysis were obtained by slow evaporation from different solvents or solvent mixtures according to their different solubility properties. **A1** was crystallized from a mixture of ethanol/methanol, after boiling the solution for 5 min and letting it cool slowly to room temperature. **A2** crystal was obtained by slow evaporation of the solvent from the saturated solution prepared using the mixture of ethanol/water. **A3** was grown from methanol using the vapor diffusion technique with diethyl ether. **B2** was crystallized by slow evaporation of the solvent from pure methanol solution, while its monohydrate form **B2·H<sub>2</sub>O** crystal was harvested from a methanol/water mixture at room temperature, respectively. **B3** was crystallized from a toluol/methanol mixture at room temperature. **B4**, **B5**, and **B8** were obtained by slow evaporation of the solvent from the solutions prepared with methanol/water mixtures. **B6** was obtained from ethanol/methanol, and **B7** was obtained from an ethanol/water mixture.

**Single-Crystal Structure Determination.** Single crystals were mounted on loops and transferred to the goniometer. X-ray diffraction data were collected at 103(2) K, except for crystals **A1** and **B3**, for which the data were measured at room temperature (293(2) K), and for **A2**, for which the temperature was set to 93(2) K. All crystals were measured on a Rigaku RAXIS-RAPID II diffractometer using Mo *K* $\alpha$  radiation (except for crystals **A3** and **B5**, for which Cu *K* $\alpha$  was used). Numerical absorption correction<sup>11</sup> has been performed on all data, except for **B7**, for which multiscan absorption correction was applied, by software CrystalClear.<sup>12</sup> Sir2014<sup>13</sup> and SHELXL<sup>14,15</sup> under WinGX<sup>16</sup> software were used for structure solution and refinement, respectively. The structures were solved by direct methods. The models were refined by full-matrix least squares on *F*<sup>2</sup>. Refinement of nonhydrogen atoms was carried out with anisotropic temperature factors. The hydrogen atomic positions were located in the different electron density maps. The hydrogen atoms that participate in intramolecular hydrogen bonds were included in the structure factor calculations to refine their positions. The isotropic displacement parameters of the hydrogen atoms were approximated from the *U*(equiv) value of the atom to which they were bonded.

Selection of data collection and refinement parameters are collected in Tables 1 and 2; all data are shown in Tables S1–S3. Structural analyses were performed with PLATON<sup>17,18</sup> software. The graphical representation and the edition of CIF files were done by Mercury<sup>19</sup> and enCIFer,<sup>20</sup> respectively. Crystal Explorer 17.5<sup>21–23</sup> was used to generate molecular Hirshfeld surfaces, two-dimensional (2D) fingerprint plots, interaction energy, and total energy frameworks<sup>24</sup> in order to visualize and analyze the intermolecular interactions in the investigated crystals. Details of the calculations can be found in the Supporting Information. The crystallographic data files have been deposited at the Cambridge Structural Database as entries CCDC 1951148–1951158.

**Aromaticity (Bird Index) Calculation.** Bird indices (*I*<sub>6</sub>)<sup>25</sup> were calculated to quantify the aromaticity of the pyridine rings. The Bird index uses bond orders instead of bond distances to calculate the aromaticity. In this way, it is possible to take into account carbon–heteroatom bonds, as well. The bond order (*N*) is calculated from the bond distances (*R*) by the Gordy formula<sup>26</sup>

$$N = \frac{a}{R^2} - b$$

where *a* and *b* are parameters calculated from the single and double bond distances of carbon–carbon or carbon–heteroatom. The *a* and *b* parameters were taken from Kotelevskii et al.,<sup>27</sup> where these data have been recalibrated using experimentally observed values of bond lengths. In our case, the bond distances (*R*) obtained by SC-XRD of the compounds were used to calculate the bond orders.

The root-mean-squared deviation of the bond orders from their arithmetic mean (*V*) was calculated and compared with those of the fully localized reference molecule (hypotetic cyclohexatrien for six-membered rings, *V*<sub>k</sub>) using the following equation

$$I_6 = 100 \times \left( 1 - \frac{V}{V_k} \right)$$

## RESULTS AND DISCUSSION

**Molecular Structures.** The crystal structures of **A1**–**A3** and **B2**–**B8** were determined by single-crystal X-ray diffraction. For comparison, the crystal structure of Form I polymorph of **B1** (4-hydroxynicotinic acid, CSD refcode KUXPUP<sup>2</sup>) was included in this study. The bond distances are collected in Table 3, and the ORTEP representations of each molecule are shown in Figure 2.

**Aromaticity and Intramolecular Hydrogen Bonding.** In the investigated HPC derivatives, the inductive effect of the positively charged N<sup>+</sup>–CH<sub>3</sub> or N<sup>+</sup>–H groups results in a highly acidic carboxylic group, the deprotonation of which occurs at very low pH levels (p*K*<sub>1</sub> < 1). In the obtained neutral (zwitterionic) form, owing to the vicinal position of the hydroxyl group to the carboxylate group, the hydroxyl proton forms an intramolecular hydrogen bond with the carboxylate oxygen. The keto–enol tautomerism of OH is well known for 4-hydroxypyridines,<sup>4,32</sup> where the ring aromaticity is lost in the keto form and pyridinone derivatives are formed, while this effect is small in 3-hydroxypyridines. In the case of the HPC derivatives, the enolic O3–H3 proton is in an intramolecular hydrogen bond with the O2 atom of the deprotonated carboxylate group (Figure S1). Whether we can speak about keto or an enol form is essentially determined by the position of the related OH proton. In the 11 investigated HPC derivatives, the electron-donating effect of the various substituents firmly modifies the electron distribution both in the aromatic ring and on the oxygen in the hydroxyl and carboxylate groups. As a result of these multiple effects, a gradual shift of the hydrogen position from the hydroxyl oxygen (enol form) to the carboxylate oxygen (keto form) was observed in the order of increasing O3–H3 distances: **A1** < **A2** < **A3** < **B2** < **B7** < **B5** < **B2·H<sub>2</sub>O** < **B3** < **B4** < **B6** < **B1** < **B8**. (The H3 proton position was refined without constraint in the crystal structure refinement processes.)

The distances of the intramolecularly bound proton from the two oxygen atoms (O3 and O2) are shown in Figure 3a. In 3HPC and 4HPC derivatives, mainly enol and keto forms were found, respectively. **B2** was the only 4HPC where the enol form was observed; however, in its hydrate crystal, the keto-form appeared (**B2·H<sub>2</sub>O**). In **B7**, the proton is located halfway between the two oxygen atoms. In the case of **B1**, Long and co-workers<sup>3</sup> found that both enol and keto forms crystallize depending on the circumstances with different arrangements and secondary interactions of the molecules.

From the three anhydrous polymorphs, the keto tautomer, Form I as **B1** (CSD refcode KUXPUP, *P*<sub>21/c</sub>, *Z'* = 1), was added to the figure, as comparison, as this crystal form gives the extreme value of the keto form in the studied series. Plotting the O2–H3 distances against the O3–H3 distances (Figure 3b), a quadratic equation can be fitted to the points, reflecting that the O2...O3 distance goes through a minimum (Table 3 and Figure S2).

Besides the proton position involved in the intramolecular hydrogen bond, the distances of nonhydrogen atoms were found to exhibit differences by the changing substituents. The bar chart in Figure 4a shows the two carboxylate bond lengths, C7–O1 and C7–O2, indicating significant differences between the 3HPC (A series) and 4HPC (B series) derivatives. While C7–O1 is clearly a double bond and C7–O2 is a single bond in 4HPC derivatives, the two bond lengths get closer to equalization in 3HPC derivatives. Considering these distances, **B2** and **B7** are closer to 3HPC than to 4HPC derivatives (Figure 4a). In the case of the keto forms, a double bond is expected between C2–C3 and C4–O3/C7. The bar chart (Figure 4b)



Table 3. Selected Bond Distances (Å) of Molecules A1–A3 and B1–B8

	A1	A2	A3	B1 <sup>a</sup>	B2	B2·H <sub>2</sub> O	B3	B4	B5	B6	B7	B8
O3–H3O	0.89(2)	1.00(4)	1.134(19)	0.942	1.11(2)	1.468(18)	1.49(3)	1.55(4)	1.45(4)	1.61(6)	1.228(16)	1.80(3)
O2–H3O	1.70(2)	1.54(4)	1.338(19)	1.619	1.35(2)	1.050(17)	1.03(3)	0.98(4)	1.04(5)	0.95(6)	1.235(16)	0.85(3)
O1–C7	1.255(2)	1.230(3)	1.230(2)	1.208(2)	1.244(2)	1.226(2)	1.207(4)	1.215(5)	1.215(5)	1.23(1)	1.236(2)	1.214(3)
O2–C7	1.244(2)	1.299(3)	1.294(2)	1.319(2)	1.292(2)	1.319(2)	1.331(4)	1.327(5)	1.333(5)	1.324(9)	1.293(1)	1.328(3)
O3–C3/C4	1.335(2)	1.348(3)	1.334(2)	1.279(2)	1.309(2)	1.285(2)	1.285(4)	1.284(4)	1.284(5)	1.30(1)	1.298(1)	1.278(3)
N1–C2	1.329(2)	1.339(3)	1.343(2)	1.343(2)	1.343(2)	1.345(2)	1.346(4)	1.343(5)	1.348(5)	1.35(1)	1.355(1)	1.350(3)
C2–C3	1.394(2)	1.403(3)	1.403(2)	1.367(2)	1.369(3)	1.371(2)	1.362(4)	1.377(5)	1.372(6)	1.37(1)	1.371(2)	1.364(3)
C3–C4	1.401(2)	1.404(3)	1.401(2)	1.437(2)	1.424(3)	1.436(2)	1.435(4)	1.435(5)	1.434(6)	1.43(1)	1.425(2)	1.435(3)
C4–C5	1.387(2)	1.389(3)	1.392(2)	1.423(2)	1.406(3)	1.423(2)	1.427(5)	1.436(5)	1.418(6)	1.40(1)	1.411(2)	1.442(3)
C5–C6	1.371(2)	1.376(4)	1.368(2)	1.345(2)	1.368(3)	1.364(2)	1.356(5)	1.360(5)	1.353(6)	1.37(1)	1.373(2)	1.364(3)
C6–N1	1.345(2)	1.344(3)	1.353(2)	1.351(2)	1.358(2)	1.370(2)	1.369(4)	1.374(5)	1.378(5)	1.39(1)	1.378(2)	1.346(3)
C3/C4–C7	1.518(2)	1.513(3)	1.517(2)	1.489(2)	1.494(3)	1.483(2)	1.483(5)	1.493(5)	1.492(6)	1.49(1)	1.497(2)	1.496(3)
N1–C8			1.477(2)				1.476(4)	1.479(5)	1.479(5)	1.49(1)	1.487(1)	
O2···O3	2.548(2)	2.492(2)	2.444(2)	2.523(2)	2.427(2)	2.475(2)	2.476(4)	2.481(3)	2.460(4)	2.502(8)	2.4310(13)	2.578(2)
bird index	90	90	87	69	79	72	68	70	69	68	75	70
pK <sub>s2</sub>	4.713(1) <sup>b</sup>	4.933(1) <sup>c</sup>	6.6326(8) <sup>d</sup>	5.955(1) <sup>a</sup>	6.32(1) <sup>e</sup>	6.32(1) <sup>e</sup>	5.9578(6) <sup>d</sup>	6.64(1) <sup>f</sup>	6.295(1) <sup>g</sup>	6.109(3) <sup>h</sup>	6.34(1) <sup>h</sup>	6.205(1) <sup>i</sup>

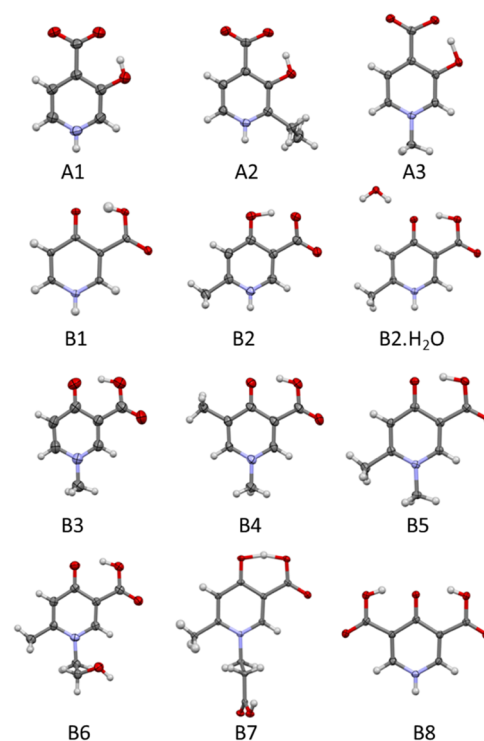
<sup>a</sup>ref 2, <sup>b</sup>ref 28, <sup>c</sup>ref 29, <sup>d</sup>ref 8, <sup>e</sup>ref 30, <sup>f</sup>ref 10, <sup>g</sup>ref 9, <sup>h</sup>ref 6, <sup>i</sup>ref 31.

Figure 2. ORTEP plot of molecules A1–A3 and B1–B8 drawn at the 50% probability level. Data for B1 (CSD refcode KUXPUP) were taken from ref 2.

shows that both bond distances are shorter in 4HPC derivatives (B series), while these bond lengths are both longer in the enolic 3HPC derivatives (A series); B2 and B7 provide a transition between the two groups.

Ring aromaticity was calculated for all compounds using the Bird index,<sup>25</sup> and the obtained values are given in Table 3. The aromaticity (Bird) index gives the root-mean-squared deviation of the bond orders in the ring in a way that this number is 100 for benzene and 0 for the fully localized hypothetical cyclohexatriene (see the Experimental Section). Lower aromaticity was found in the 4HPC derivatives, where this value falls in the range of 68–73, while it increased to 75 and 79 in B7 and B2, respectively (Table 3). The highest values were calculated in the case of 3HPC derivatives, where this value ranged between 87 and 90. A significant correlation ( $R = 0.9159$ ) was found between the O2–H3 distances and the calculated Bird index, showing that higher aromaticity corresponds to an increasing distance of the proton from the carboxylate oxygen (enolic form develops, Figure 5).

At the same time, the distance between the ring carbon and the hydroxyl oxygen (C<sub>ring</sub>–O3 bond) also shows a positive correlation with the calculated aromaticity index (Figure S3). It can also be concluded that 4HPC derivatives are not necessarily in an immoderate keto form if electron-donating ring substituents increase the electron density on the hydroxyl oxygen, as in the case of the 6-methyl-substituted B2 and 6-methyl-1-carboxyethyl-substituted B7.

**Packing Arrangements.** We examined how the molecular arrangement and interactions are affected by the proton donor and acceptor substituents on the pyridine ring in the crystals. The packing arrangements viewed from the *a*, *b*, and *c* crystallographic axis directions are collected in Figures S4–S6 for the investigated crystals. In order to be able to perform crystal engineering, it is important to understand the

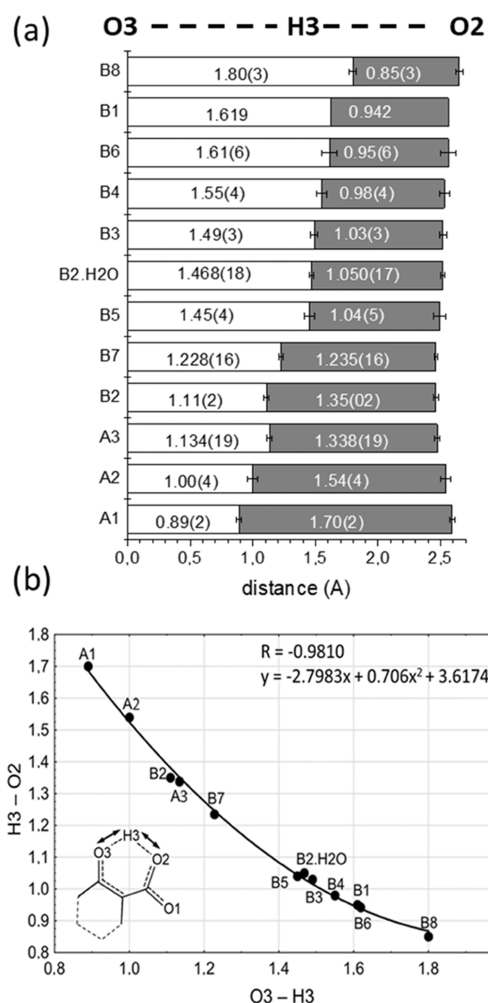


**Figure 3.** Position of the proton involved in intramolecular hydrogen bonding between the hydroxyl (O3) and carboxylate (O2) oxygen atoms plotted in the (a) column diagram and in (b) *xy* diagram. Data for **B1** were taken from ref 2.

intermolecular interactions and recognition phenomena in the context of supramolecular structures. Synthons are constructed from designed combinations of interactions, which means that synthons incorporate both electrostatic and sterical recognition features of molecular fragments.<sup>33,34</sup>

**Stacking Arrangements between the Planar Molecules.** In all investigated HPC derivatives, owing to their relatively planar geometry and in the absence of spacious but polarizing functional groups, significant C–O $\cdots\pi$  or  $\pi\cdots\pi$  (off-center parallel stacking) interactions are present. The arrangements of the molecules are shown in Figure 6, and the characteristic geometric parameters describing these interactions are collected in Table 4. The C–O $\cdots\pi$  interactions with the participation of the carboxylate oxygen atoms could be found in crystals of **A1**, **A3**, **B7**, and **B8**. Similar interactions but with the participation of hydroxyl oxygen could be found in **B3** and **B6**: this is in agreement with the previously established electronic differences between 3HPC and 4HPC derivatives. The shortest C–O $\cdots\pi$  interaction of 3.2745(15) Å was detected in crystal **A1**. Significant stacking interaction (with a distance < 4.0 Å) between neighboring pyridine rings was found in crystals **A2**, **B2**·H<sub>2</sub>O, and **B3**–**B7**. In the case of **B2**, the distance between the parallel molecules (arranged below and above each other) is rather far, 4.7412(12) Å, while short C–O $\cdots\pi$  interaction with a

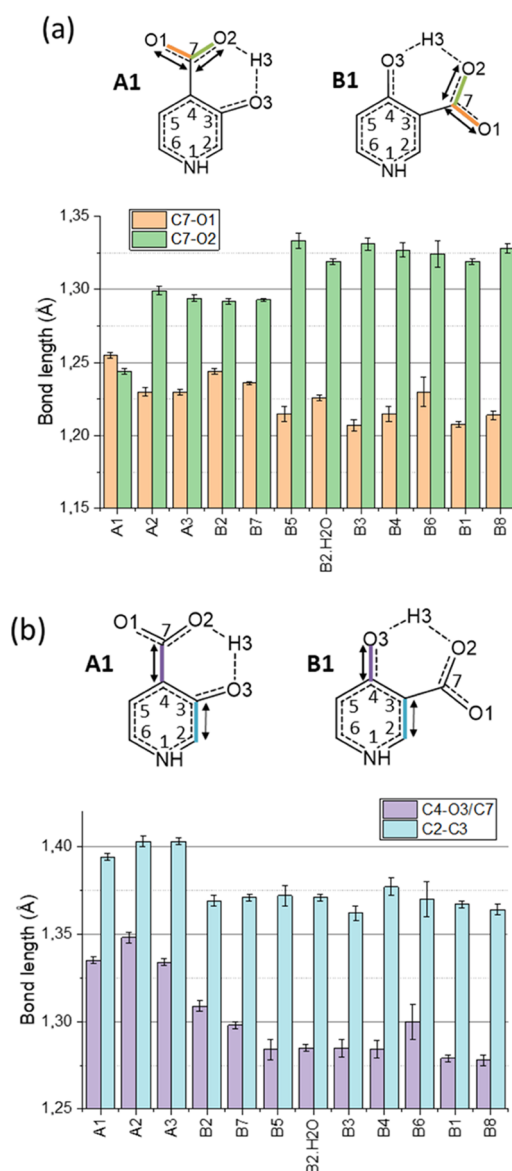


**Figure 4.** Bar charts for the selected nonhydrogen bond distances (Å): (a) C7–O2 and C7–O1 and (b) C4–O3/C7 and C2–C3. Diagrams of formulas of **A1** and **B1** show the investigated bond distances with atom numbering.

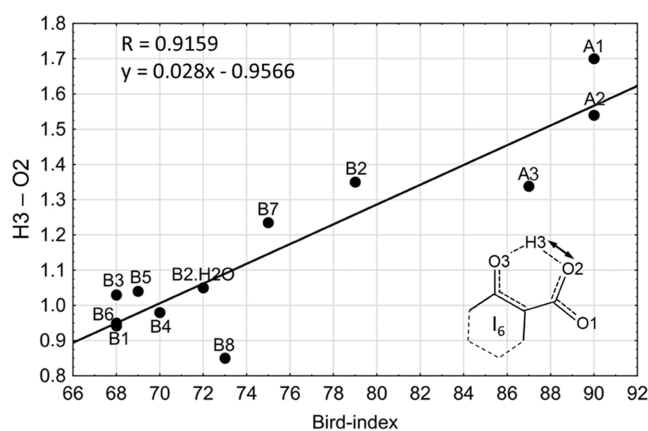


**Figure 5.** Correlation between O2–H3 distances and the calculated Bird index (*I*<sub>6</sub>) values.

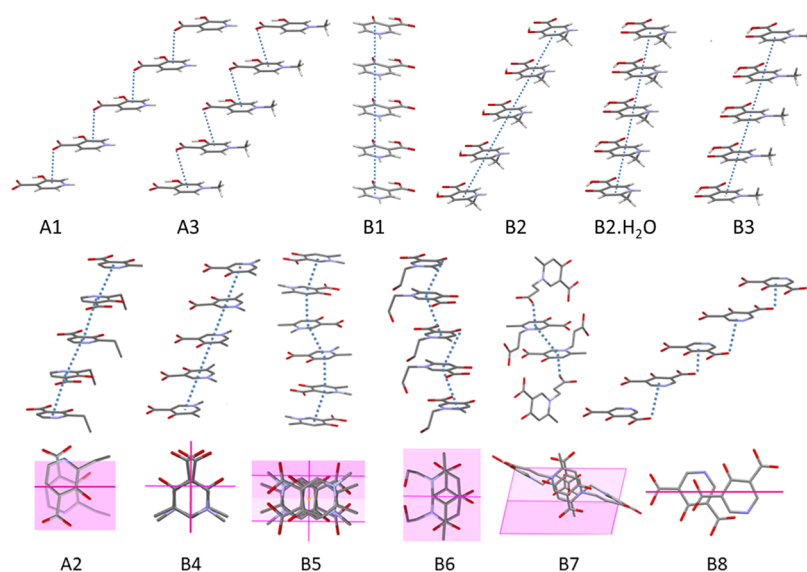


**Figure 6.** Stacking arrangement of the HPC derivatives showing the C–O...Cg and Cg...Cg interactions. The symmetry elements appear in the colors viewed from the direction of the pyridine rings. Data for **B1** were taken from ref 2.

**Table 4.** Selected Distances and Angles Related to C–O... $\pi$  and  $\pi$ ... $\pi$  Interactions in Crystals **A1–A3** and **B1–B8**<sup>a,b7</sup>

comp.	C–O...Cg	O...Cg (Å)	C–O...Cg (°)	C...Cg (Å)	symmetry code	
<b>A1</b>	C7–O1...Cg(1)	3.4512(13)	111.30(10)	4.0780(18)	1 + X, Y, Z	
	C7–O2...Cg(1)	3.2745(15)	96.21(10)	3.6263(17)	X, –1 + Y, Z	
<b>A3</b>	C7–O2...Cg(1)	3.296(2)	126.64(2)	4.199(2)	X, 1/2 – Y, –1/2 + Z	
<b>B2</b>	C7–O2...Cg(1)	3.373(3)	138.24(2)	4.421(3)	1/2 – X, –1/2 + Y, 1/2 – Z	
<b>B3</b>	C4–O3...Cg(1)	3.990(3)	68.27(2)	3.711(3)	–1 + X, Y, Z	
<b>B6</b>	C4–O3...Cg(1)	3.756(8)	67.7(4)	3.476(9)	1/2 + X, 1/2 – Y, Z	
<b>B7</b>	C10–O5...Cg(1)	3.6127(11)	67.86(7)	3.3496(13)	X, 1/2 – Y, –1/2 + Z	
<b>B8</b>	C7–O1...Cg(1)	3.6152(18)	69.20(14)	3.380(3)	–1/2 + X, 1/2 – Y, –1/2 + Z	
	Cg(I)...Cg(J)	Cg...Cg (Å)	CgI_Perp (Å)	$\alpha$ (°)	offset (Å)	symmetry code
<b>A2</b>	Cg(1)...Cg(1)	3.8962(13)	3.3553(9)	0.91(11)	1.944	1/2 – X, –1/2 + Y, Z
<b>B1</b>	Cg(1)...Cg(1)	3.804(3)	3.3340(7)	0.00(8)	1.8969	–1 + X, Y, Z
<b>B2</b>	Cg(1)...Cg(1)	4.7412(12)	3.1651(8)	0.00(9)	3.53	–1 + X, Y, Z
<b>B2·H<sub>2</sub>O</b>	Cg(1)...Cg(1)	3.7841(8)	3.3506(5)	0.03(6)	1.759	–1 + X, Y, Z
<b>B3</b>	Cg(1)...Cg(1)	3.893(2)	3.4833(12)	0.02(14)	1.739	–1 + X, Y, Z
<b>B4</b>	Cg(1)...Cg(1)	3.702(2)	3.3936(15)	0.80(17)	1.478	1/2 – X, Y, –1/2 + Z
<b>B5</b>	Cg(1)...Cg(1)	3.460(2)	3.2970(17)	8.2(2)	1.057	3/2 – X, 1/2 – Y, Z
	Cg(1)...Cg(1)	3.521(2)	3.2278(17)	0.0(2)	1.418	1 – X, 1 – Y, –Z
<b>B6</b>	Cg(1)...Cg(1)	3.706(5)	3.305(3)	1.6(4)	1.592	–1/2 + X, 1/2 – Y, Z
<b>B7</b>	Cg(1)...Cg(1)	3.9674(8)	3.3164(5)	0.00(5)	2.178	1 – X, –Y, 1 – Z

<sup>a</sup>Ring (1) is the pyridine ring. Cg(1)...Cg(1): distance between ring Centroids (Å), Cg(1)\_Perp: perpendicular distance of Cg(1) on neighbouring ring (Å),  $\alpha$ : Dihedral angle between planes (°). <sup>b</sup>Data for **B1** were taken from ref 7.

distance of 3.373 Å is found. The shortest ring centroid Cg...Cg distance of 3.460(2) Å is measured in crystal **B5**. Steric effects can also be observed in these lattices in addition to electronic effects. If there is no or only one methyl group on the pyridine ring, the molecules are arranged one below the other with a simple offset (see crystals **A1**, **A3**, **B1**, **B2**, **B2·H<sub>2</sub>O**, and **B3** in Figure 6), probably because the adjacent methyl hydrogen atoms are located sufficiently apart in these lattices. If more than one methyl group or longer substituents are introduced into the ring, in addition to the translation, glide planes, perpendicular to the pyridine ring planes, mirror the molecules in **A2**, **B4**, **B5**, **B6**, **B7**, and **B8**. Figure 6 (second row) shows the symmetry elements that appear in these crystals. In the case of the large carboxyethyl substituent (**B7**), the stacking interaction is limited to dimers instead of columns and the interactions are completed

by C9–H9A...O3 and C9–H9B...O2 hydrogen bonds (Table S1).

**H-Bonding Interactions.** The Hirshfeld surface<sup>21</sup> of the molecules was calculated to interpret and compare their arrangement in their crystal lattices influenced by secondary interaction. The Hirshfeld surface is defined by the density weight function of the selected molecule over the same sum of the density of its nearest neighbors. The obtained isosurface provides information about intermolecular interactions (see the Supporting Information). The calculated Hirshfeld surfaces and neighboring molecules with N/C–H...O connections are shown in Figures 7 and 8. The electron distribution of HPC derivatives is such that a partial negative charge is created on the oxygen-containing functional groups, while a partial positive charge is created on the protonated or methylated pyridine



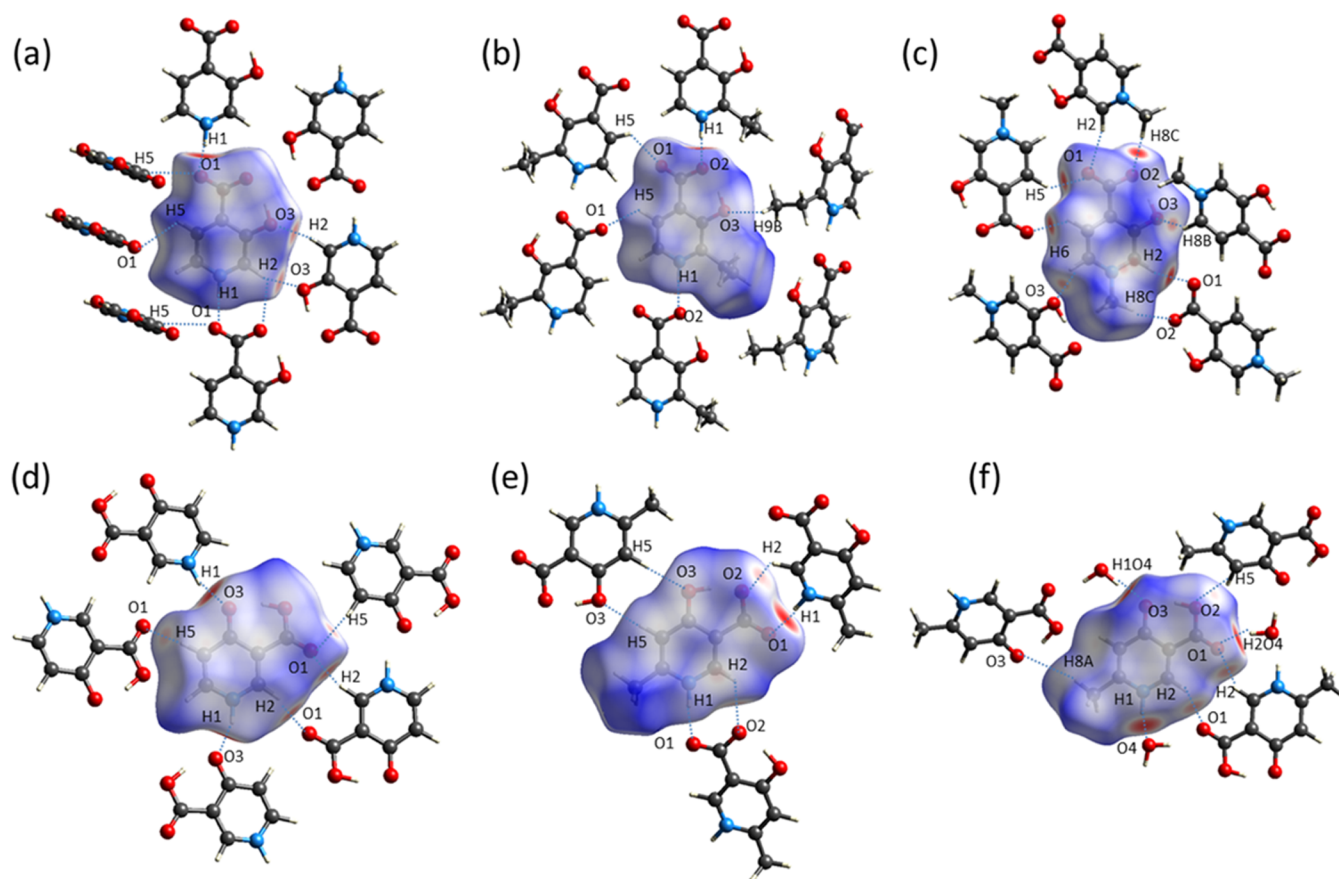


**Figure 7.** Hirshfeld surfaces and H-bond connections around one selected molecule in crystals (a) A1, (b) A2, (c) A3, (d) B1, (e) B2, and (f) B2·H<sub>2</sub>O.

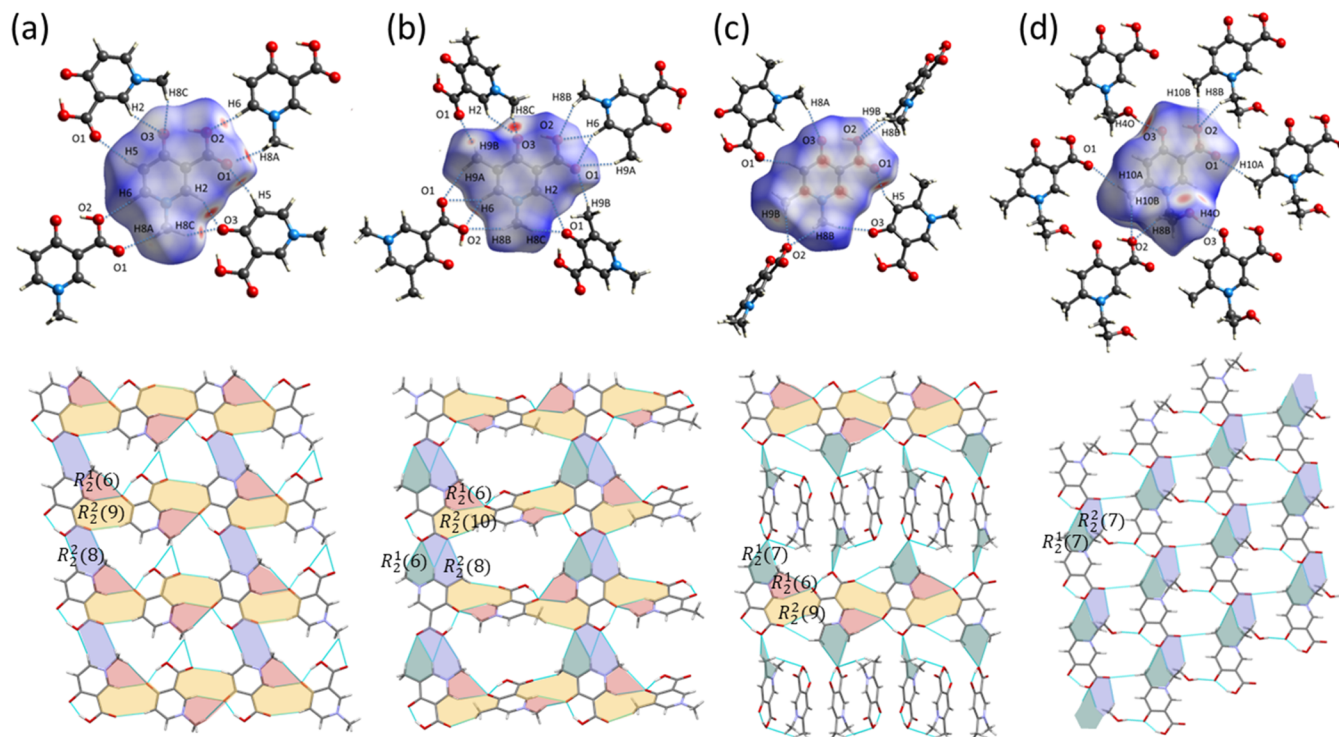


**Figure 8.** Hirshfeld surfaces and H-bond connections around one selected molecule (up) and packing arrangements with colored areas showing similar synthons (bottom) in crystals (a) B3, (b) B4, (c) B5, and (d) B6. Graph set descriptors are indicated.

nitrogen. This helps the molecules to arrange themselves in rows in the plane of the pyridine rings with hydrogen bonds by N—

H $\cdots$ O and C–H $\cdots$ O interactions. The primary driving force in the molecular arrangement is the formation of hydrogen bonds

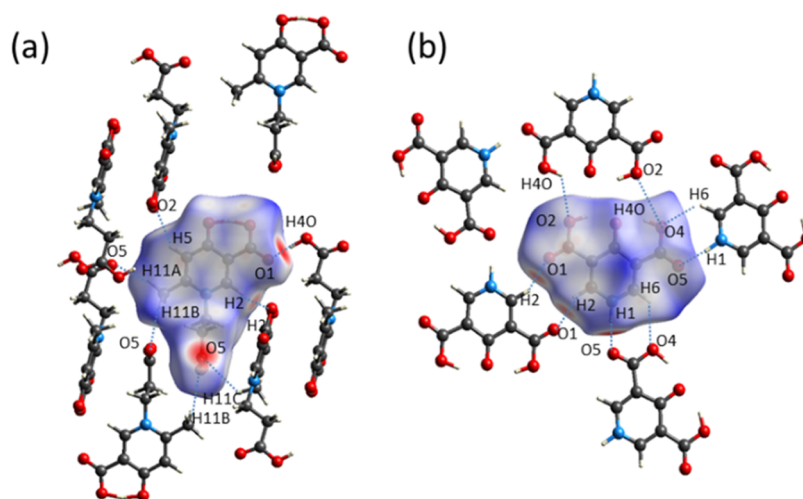


**Figure 9.** Hirshfeld surfaces and H-bonding connections around one selected molecule in crystals (a) B7 and (b) B8.

between the positively charged N–H or N–CH<sub>3</sub> groups and the negatively charged oxygen atoms. H-bond distances and angles of the main intermolecular interactions in all investigated crystals are collected in Table S4.

N1–H1 is connected to carboxylate O1 in crystal A1, while to the carboxylate O2 oxygen in A2, and this type of interaction continues forming a chain of molecules in these crystals (A1, double chain in the *ab* diagonal having a symmetry center, see Figure 7a; A2, sheet in the *ab* plane, see Figure 7b). By graph set description,<sup>35</sup> this chain is described as C<sub>1</sub><sup>i</sup> (7), where C<sub>D</sub><sup>A</sup> (N) shows the number of acceptor atoms (A), donor atoms (D), and the number of atoms in the repeating unit of the chain (N). In A3, the H8C hydrogen atom from the N–CH<sub>3</sub> group connects carboxylate O2, and neighboring ring hydrogen atom H2 is in weak interaction with O1, which eliminates the straight chain structure and replaces it with a ring R<sub>2</sub><sup>2</sup> (8) (Figure 7c). The hydroxyl O3 connects to ring hydrogen atoms H2 and H8B, respectively, in A1 and A3 and to ethyl side chain hydrogen atom H9B in A2. Unlike A1–A3, in crystal B1 (CSD refcode KUXPUP<sup>2</sup>), the electron distribution on the oxygen atoms is reversed, which is expressed in the fact that the NH group binds to the hydroxyl O3 oxygen instead of the carboxylate oxygens; however, the linear chain is formed and described here as C<sub>1</sub><sup>i</sup> (6), a simple chain organized by the glide plane along the *c*-axis (Figure 7d). Carboxylate oxygen O1 forms a dimer through C2–H2...O1 connection and vice versa with a neighboring molecule, forming an R<sub>2</sub><sup>2</sup> (10) ring motif (Figure 7d).

In most of the 4HPC derivatives, the keto form is favored, which means that the H3 proton is bonded to the carboxylate O2 atom. Molecule B2 was able to be crystallized in its hydrate form B2·H<sub>2</sub>O and the expected keto form was found, but the enol form was detected in the anhydrous B2 crystal (see Figure 2 and Figure 7e,f). Presumably, the reason for this is that the positive inductive effect of the 6-methyl group equalizes the electron density on the O2 and O3 oxygen atoms in B2; thus, both the keto and enol forms can be stabilized in certain crystals. In the hydrate form, the B2 molecule is surrounded by three water molecules of crystallization and involved in the hydrogen bonds O4–H1O4...O3, O4–H2O4...O1, and N1–H1...O4 (Figure 7f). These intermolecular interactions shift the partial charges in the oxygen atoms in the carboxyl moiety, and in this way, the intramolecularly bound hydrogen is transferred to the O2 atom. The N1–H1 bonds to carboxylate O1 in B2 and to a

water oxygen in B2·H<sub>2</sub>O also contribute to the differently polarized environment. On the other side of the molecule, a dimer is formed via the C5–H5...O3 bond around a symmetry center in B2 (R<sub>2</sub><sup>2</sup> (7)) and via the C2–H2...O1 bond in B2·H<sub>2</sub>O (R<sub>2</sub><sup>2</sup> (10)). This latter synthon is the same as in B1 (Figure 7d).

Both keto and enol tautomers could be crystallized only for this non-*N*-methylated compound (B2), depending on the presence or absence of water of crystallization. The observed findings support the previous statements of Long et al.,<sup>3</sup> that the molecule prefers to crystallize in the keto form in a polarized environment. Since no similar tautomerization was found in the crystal structure of any other investigated *N*-methyl derivatives, we can assume that the electron distribution can be influenced much more easily by the intermolecular interaction with neighboring molecules in the N–H than in the N–CH<sub>3</sub> pyridine derivatives. The four *N*-methyl 4HPC derivatives, namely, 1-methyl (B3), 1,5-dimethyl (B4), 1,6-dimethyl (B5), and 1-(2-hydroxyethyl)-6-methyl (B6), have similar synthons and thus packing arrangements in certain directions (Figure 8).

These molecules have relatively positive N–CH<sub>3</sub> and negatively charged oxygen-rich parts. The main intermolecular interactions are C–H...O-type interactions between the molecular sections of opposite polarity, thus creating similar molecular arrangements. The similar synthons in the different structures are presented in Figure 8 with areas of the same color. The summary of O–H...O intra- and C–H...O intermolecular interactions is listed in Table S5. In the *N*-methylated compounds, the N–CH<sub>3</sub> group is connected to the hydroxyl O3 atom in each case, which has the highest electron density (see C8–H8C...O3 in Figure 8a,b and C8–H8A...O3 in Figure 8c). The neighboring ring hydrogen atom H2 also comes close to O3, and the carboxylate O1 is able to interact with H5 ring hydrogen atoms in B3 and B5 and with methyl hydrogen atom H9B in B4. This means that despite methylation on 5- or 6-positions in B4 and B5, respectively, the main interactions of B3 are preserved in the crystals of B4 and B5 in this direction (see also the yellow and pink areas in Figure 8a–c). The *N*-methyl hydrogen atoms can take over the role of the H-donor from ring hydrogen atoms without causing steric hindrance. The adjacent pyridine rings involved in this synthon interaction are almost parallel in B3 and B5 (the angles between neighboring pyridine ring planes are 5.2 and 8.0°, respectively), while the ring planes turn by 47.1° in B4. In the transverse direction of the described

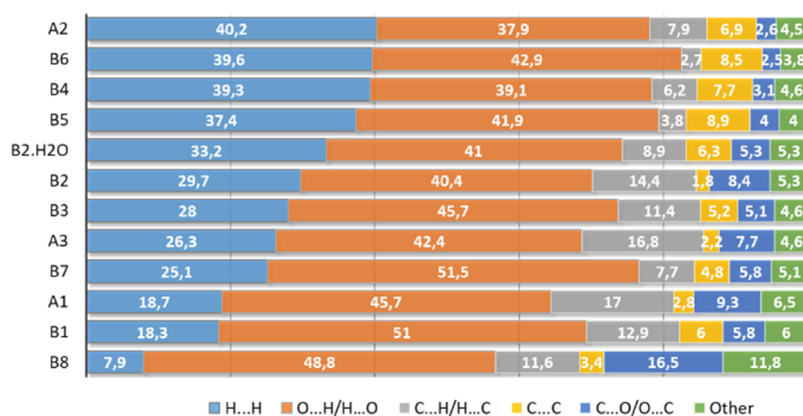


**Figure 10.** Relative contribution of different secondary interactions to the Hirshfeld surface area.

column, another hydrogen-bonding system is built in **B3–B5** with the contribution of the two carboxylate oxygen atoms O1 and O2 bonding to N–CH<sub>3</sub> hydrogen atoms, ring hydrogen atom H6, and methyl hydrogen atoms on C9 if it is present (Figure 8a–c). In the case of **B3**, the adjacent rings are parallel in this direction with a distance of 1.386 Å between the planes (the Cg...Cg distance is 8.104(2) Å). In **B4**, the neighboring ring planes are also very close to being parallel with an angle of 0.8°. However, they are almost perpendicular in **B5** with an angle of 79.7° (see also the purple and green areas in Figure 8a–c). In the case of **B6**, the presence of the hydroxyethyl side-chain modifies the arrangements of the molecules compared with **B3–B5**, as the side-chain OH hydrogen atom is connected to neighboring OH3 atom and their pyridine ring planes are parallel to each other with a distance of 1.680 Å (the Cg...Cg distance is 8.249(2) Å). In this crystal, a third chain emerges by the contribution of C10–H10A...O1 interaction with the rotation of the adjacent molecules by 23.6° (Figure 8d). Nevertheless, concerning the synthons shown by green and blue areas in Figure 8d, the arrangement of the molecules is similar to **B4**.

In **B7**, a carboxyethyl side chain is introduced to the pyridine nitrogen. It was able to completely change the previously presented system of synthons. Two molecules form a dimer with an offset parallel stacking (see Table 4) accompanied by C9–H9B...O2 and C9–H9A...O3 H-bonding interactions (Table S5 and Figure 9a).

Neighboring dimers are placed perpendicular to each other with the O4–H4O...O1 and C2–H2...O3 interactions. In the other direction, the side-chain carboxylate oxygen O5 is connected to the methyl hydrogen atom H11A (Table S5 and Figure 9a). In **B8**, the second carboxylate group on the pyridine ring, similarly to the first one, is in the meta position to the hydroxyl group, and both are in an intramolecular H-bond with it. Turning face to face with these functional groups, a dimer is formed via O4–H4O...O2 around the symmetry center (Figure 9b). Due to the flat molecular structure, layers are formed by C–O...Cg interactions (Table 4). Within a layer, the molecules are connected by N/C–H...O interactions (N1–H1...O5, C6–H6...O4, C2–H2...O1, Table S5).

**Ratio of the Different Secondary Interactions Based on Hirshfeld Surface Analysis.** Hirshfeld surface analysis provides information about the relative contribution of the different types of secondary interactions to the overall intermolecular interactions in a crystal. 2D fingerprint plots were calculated to get this quantitative information on the supramolecular interactions (Figures S7 and S8). The obtained ratio (%) of the

specific interactions contributing to the Hirshfeld surface area is collected in Table S6. These data are represented in the order of growing H...H contacts in Figure 10. It can be seen that the ratio of H...H contacts is the lowest in **B8**, where a second carboxyl group is present on the pyridine ring. This also means that, at the same time, the ratio of its O...H contacts is one of the highest in the series. The C...O/O...C contact ratio is also the highest in **B8** because of the strong C–O...Cg interactions occurring in the crystal.

**A1** and **B1** are unsubstituted 3HPC and 4HPC, respectively. They have the same molecular shape; only the position of the nitrogen atom in the pyridine ring differs. It provides an excellent opportunity for a structural comparison, as the steric effects can be neglected, and electronic differences dominate the molecular arrangements. Their H...H ratios are almost equal; however, the O...H/H...O and C...C contact ratios are higher in **B1**, while C...H/H...C and C...O/O...C contact ratios are higher in **A1**, which is in agreement with the shorter  $\pi\cdots\pi$  distances in **B1** and C–O... $\pi$  distances obtained in **A1** (Table 4). This can be explained by the different arrangements of the molecules: in **B1**, the molecules form parallel layers, while they have perpendicular arrangements in **A1**. Compound **B7** with the carboxyethyl side chain resulted in the highest proportion of O...H/H...O contacts among the investigated crystals. The next two compounds in the ascending order of H...H contacts are the *N*-methylated 3HPC **A3** and 4HPC **B3**; in their cases, the H...H contact ratios are very close, and the difference between the contributions of the other interactions is very similar to that of **B1** and **A1**. It can be observed again that the molecular arrangements are parallel in **B3** and perpendicular in **A3**. Comparing the data of the Hirshfeld calculation of the anhydrous and hydrate forms of **B2**, surprisingly, the H...H ratio is somewhat higher for the hydrate form. The O...H/H...O ratio is very similar, and the differences in C...H/H...C, C...O/O...C, and C...C contacts can probably trace back to the stronger  $\pi\cdots\pi$  interactions in **B2**·H<sub>2</sub>O vs the C–O... $\pi$  in **B2**. Compounds **B4**, **B5**, and **B6** all contain an *N*-methyl group and another methyl substituent on the pyridyl ring, and they showed very similar synthon arrangements in their crystals. This similarity is also reflected in the proportions of their secondary interactions shown in Figure 10. Finally, compound **A2**, which contains an ethyl group, possesses the highest H...H and lowest O...H/H...O relative contribution to the Hirshfeld surface area, indicating that this extra substituent changes the ratio of secondary interactions very significantly compared to non-substituted compound **A1**.



**Interaction Energy and Energy Frameworks.** The two pairs of compounds **A1/B1** and **A3/B3** from the investigated series have the same molecular shape, but their electron distribution differs due to the different nitrogen positions in the pyridine ring. This gave us the opportunity to examine how the difference in electron distribution only and exclusively affects the arrangements of the molecules. For comparison, all the other anhydrous polymorphs of **B1**, i.e., Form I (CSD refcode KUXPUP<sup>2</sup>), Form II (CSD refcode KUXPUP01<sup>3</sup>), and Form III (CSD refcode AKIHAF<sup>3</sup>), were involved into this investigation with **A1**. Furthermore, **B2** was also examined together with **A3** and **B3**, which contain the same substituents but are in different positions, giving another comparable group for this energetic study. First, the electrostatic potential was calculated and mapped over the Hirshfeld surface to compare the differences in the electron distribution. Then, the calculation of pairwise interaction energies within the crystal was performed by summing up four energy components comprising electrostatic ( $E_{\text{ele}}$ ), polarization ( $E_{\text{pol}}$ ), dispersion ( $E_{\text{dis}}$ ), and repulsion ( $E_{\text{rep}}$ ) and using the B3LYP/6-31G(d,p) energy model. For this energy calculation, molecules within 3.8 Å of a reference molecule have been taken into account. In the case of AKIHAF, where two independent molecules are in the asymmetric unit, the calculation was performed in two consecutive steps for molecule 1 and then for molecule 2 to get all independent intermolecular energies. Results obtained for **A1**, KUXPUP, KUXPUP01, and AKIHAF are shown in Figure 11. The calculated pairwise interaction energies with color codes are collected for comparison in Table S7.

Although the molecular shapes of **A1**, KUXPUP, KUXPUP01, and AKIHAF are the same, their calculated Hirshfeld surfaces showing the electrostatic potential (Figure 11a) are different due to the altered arrangement of the pyridine nitrogen atoms and neighboring molecules. The most negative area is marked in red around the carboxylate oxygen atoms. In KUXPUP and KUXPUP01, there is a strong red spot at the hydroxyl oxygen atoms since this oxygen is deprotonated. The most positive area, marked by blue, is around the hydrogen atom of the pyridine nitrogen in all four cases, which is in para position to the carboxylate group in **A1** and meta position in the case of all **B1** polymorphs. The different directionality of the positive charges within the molecule favors the linear arrangements of the neighboring molecules due to N–H...O bonds in the former case, while the N–H...O bonds are in an angle versus the carboxylate groups in the **B1** polymorphs (Figure 11b). The calculated total intermolecular energies were the strongest in these directions in the case of **A1** with the molecule in green (−106.1 kJ/mol) and in the case of AKIHAF with the molecule in magenta (−99.3 kJ/mol). In KUXPUP, a dimer is formed with the adjacent molecule in light blue, with an interaction energy of −64.1 kJ/mol. In the case of KUXPUP, the N–H and neighboring C–H connect to the carboxylate oxygen atoms, forming a ring with a neighboring molecule in magenta, with an interaction energy of −62.6 kJ/mol. The energy frameworks were calculated for a cluster to enhance the topology comparison of the overall interaction energies among the molecules in the crystals. The importance of this functionality is more pronounced in the case of polymorphs as it allows users to directly compare the topological differences of the energy components among the structures, which may be correlated with physicochemical properties. In our cases, the topology of the total energy is significantly governed by electrostatic forces, and their directionality differs considerably due to the different

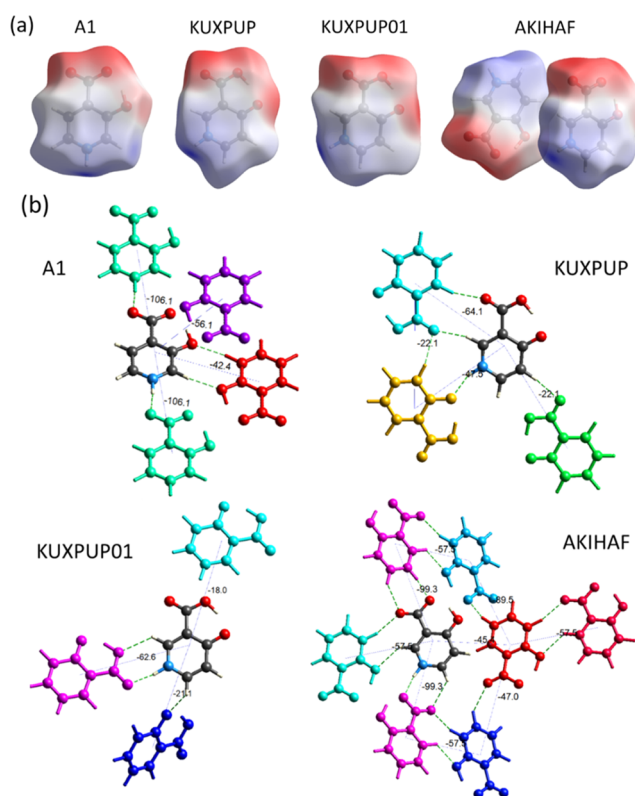


**Figure 11.** (a) View of the calculated electrostatic potentials of **A1** and various **B1** polymorphs, namely, Form I (CSD refcode KUXPUP), Form II (CSD refcode KUXPUP01), and Form III (CSD refcode AKIHAF), mapped over the Hirshfeld surface. Red and blue regions represent negative and positive electrostatic potentials, respectively. (b) Color-coded interaction mapping within 3.8 Å of the reference molecule with the calculated  $E_{\text{tot}}$  values between selected molecular pairs (data are collected in Table S6).

molecular arrangements in the four crystals. The directions of main forces show linear columns, hexagonal rings, crosses, and zigzag forms in **A1**, KUXPUP, KUXPUP01, and AKIHAF, respectively (Figure S9). Based on the above, we can draw the conclusion that a similar shape does not result in a similar arrangement of these small, near-spherical molecules. Instead, the charge distribution within the molecule determines the direction of supramolecular interactions with the neighboring molecules. Vice versa, intermolecular interactions may also influence the electron distribution of the molecule in the crystal. In this compound family, it affects the position of the hydrogen atom, determining whether an enol or a keto tautomer is formed.

In the case of methyl derivatives, **B2**, **A3**, and **B3**, the obtained pairwise interaction energies with color codes are collected in Table S8, and the electrostatic potential surfaces together with selected interactions with the reference molecules are shown in Figure S10. Owing to the position of the *N*-methyl groups, the molecular shape and thus the electrostatic potential surface are elongated in **B2** and **A3**, while they are curved in **B3** (Figure S10a). In all three cases, the electrostatic potential shows the strongest negative values around the carboxylate group (Figure S10a), while the positive part is located at the opposite end of the molecule close to the pyridine N–H or N–CH<sub>3</sub> groups. In the case of **B2** and **A3**, the negative molecular part containing the acceptor O atoms is connected to the positive molecular part of N–H or C–H hydrogen atoms at the side of the molecule, which causes the acceptor molecule to be located along its

length, while the donor molecule takes a direction perpendicular to it (Figure S10b). The energies calculated for this interaction were  $-64.9$  kJ/mol for **B2** (green molecule in the figure) and  $-49.7$  kJ/mol for **A3** (dark blue molecule). Another similarity between the molecular arrangements in **B2** and **A3** is that we calculated a strong  $\pi\cdots\pi$  interaction energy between the selected molecule and the neighboring molecule taking the opposite direction (light green molecule for **B2** with energy of  $-57.7$  kJ/mol, and light blue with  $-93.9$  kJ/mol for **A3**, see Figure S10b). In **B3**, the strongest interaction of the reference molecule was found with an adjacent molecule with which three C–H $\cdots$ O interactions are formed with a calculated energy value of  $-41.3$  kJ/mol (yellow molecule in Figure S10b).

By comparing the electrostatic potential force, dispersion force, and total energy frameworks calculated for their clusters of  $3 \times 3 \times 3$  unit cells, we can see similar hexagonal shape topology in the case of **B2** and **A3** (Figure 12).

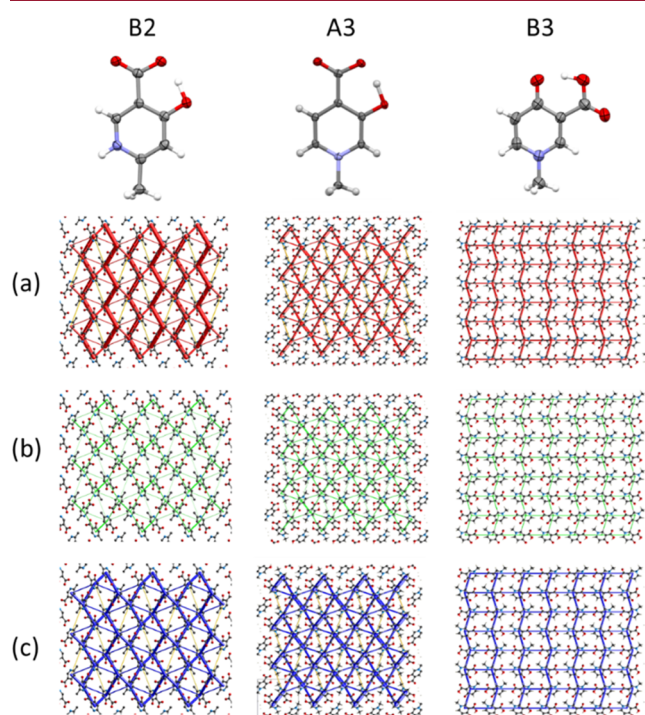


**Figure 12.** Energy frameworks calculated for a cluster of  $3 \times 3 \times 3$  unit cells of **B2**, **A3**, and **B3** viewed along the crystal axis, showing the (a) electrostatic potential force, (b) dispersion force, and (c) total energy diagrams. The cylindrical radii are proportional to the relative strength of the corresponding energies, and they were adjusted to the same scale factor of 60 with a cutoff value of 9 kJ/mol.

This is probably due to the similarities described above, originating from the similar locations of the positive and negative regions within the molecules, even though the pyridine nitrogen position differs in the two compounds. The direction of the synthons formed by the hydrogen-bonding system arranges the molecules in a similar hexagonal shape. The slightly curved **B3** differs both in its shape and electron distribution, so its topology is also different from the previous two crystals. We can say that the incorporation of the methyl group on the pyridine ring (in **A3**, **B2**, and **B3**) increased the effect of the molecular shape on the crystal packing compared with the **A1** and **B1** basic compounds.

## CONCLUSIONS

The gradual aromaticity changes and their effects on keto–enol tautomerism, packing arrangements, and secondary interactions were investigated in a hydroxypyridine-carboxylate (HPC) compound family involving three 3HPC and eight 4HPC derivatives. In their neutral (zwitterionic) forms, the OH proton forms an intramolecular hydrogen bond with the deprotonated carboxylate group. The position of this proton is gradually shifted in the investigated compounds between the enol and keto forms. In 3HPC derivatives, enol forms were found, and in 4HPC derivatives, mainly keto forms were found. **B2** was the only 4HPC where the enol form was observed; however, in its hydrate crystal (**B2**·H<sub>2</sub>O), the keto form appeared. In **B7**, the proton was located halfway between the two oxygen atoms; therefore, it could not be clearly assigned to the keto or enol form. The aromaticity of the compounds was quantified using the Bird index calculated from the distance between the ring atoms. A significant correlation ( $R = 0.9159$ ) was found between the carboxylate oxygen–proton distances and the calculated Bird indexes, showing that increasing aromaticity comes along with formation of the enolic tautomer. It is also concluded that 4HPC derivatives are not necessarily in the keto form if electron-donating ring substituents are present in the 6-position, which was the case for 6-methyl-substituted **B2** and 1-(2-carboxyethyl)-6-methyl-substituted **B7**.

In all investigated HPC derivatives, owing to their relatively planar molecular geometry, significant C–O $\cdots$  ring or  $\pi\cdots\pi$  (off-center parallel stacking) interactions arrange the molecules into columns. If there is no methyl group or only one methyl group on the pyridine ring, the molecules are arranged one below the other with an offset. If more than one methyl group or longer substituent on the pyridine ring is present, in addition to the translation, glide planes also occur perpendicular to the pyridine ring, presumably to avoid the proximity of the side chains.

The main hydrogen-bonding networks were also investigated. In the HPC derivatives, a partial negative charge is present on the oxygen atoms, while a partial positive charge is located on the proton or methyl group bonded to the pyridine nitrogen. This electronic distribution arranges the molecules into rows in the plane of the pyridine rings with hydrogen bonds of strong N–H $\cdots$ O and C–H $\cdots$ O types. Despite substitution on 5- or 6-positions in **B4**–**B6**, the main H-bonding interactions (synthons) of **B3** are preserved in their crystals.

With the help of pairwise interaction energies and total energy frameworks, the unsubstituted compounds (**A1** and polymorphs of **B1** (KUXPUP, KUXPUP01, and AKIHAF)) and one-methylated compounds **A3**, **B2**, and **B3** were compared with each other. Based on the same molecular shape but different electron distributions, the effects of shape on the arrangement of the molecules could be ruled out, and electronic forces could be exclusively studied. We can draw the conclusion that in the case of small spherical molecules (e.g., **A1** or **B1**), the charge distribution within the molecule determines the direction of supramolecular interactions. Incorporation of the methyl substituent on the ring (in the case of **A3**, **B2**, and **B3**) prioritized the effect of the molecular shape on the arrangement of the molecules in their crystals by changing the directionality of the intermolecular interactions.



## ■ ASSOCIATED CONTENT

### Supporting Information

The Supporting Information is available free of charge at <https://pubs.acs.org/doi/10.1021/acs.cgd.3c01118>.

X-ray crystallographic data; packing arrangements; H-bond distances and angles; 2D fingerprint plots of the Hirshfeld surfaces, and energy framework calculations (PDF)

### Accession Codes

CCDC 1951148–1951158 contain the supplementary crystallographic data for this paper. These data can be obtained free of charge via [www.ccdc.cam.ac.uk/data\\_request/cif](http://www.ccdc.cam.ac.uk/data_request/cif), or by emailing [data\\_request@ccdc.cam.ac.uk](mailto:data_request@ccdc.cam.ac.uk), or by contacting The Cambridge Crystallographic Data Centre, 12 Union Road, Cambridge CB2 1EZ, UK; fax: +44 1223 336033.

## ■ AUTHOR INFORMATION

### Corresponding Author

Nóra V. May – Centre for Structural Sciences, HUN-REN Research Centre for Natural Sciences, H-1117 Budapest, Hungary; [orcid.org/0000-0003-4770-4681](https://orcid.org/0000-0003-4770-4681); Email: [may.nora@ttk.hu](mailto:may.nora@ttk.hu)

### Authors

G. Tamás Gál – Centre for Structural Sciences, HUN-REN Research Centre for Natural Sciences, H-1117 Budapest, Hungary

Tamás Holczbauer – Centre for Structural Sciences, HUN-REN Research Centre for Natural Sciences, H-1117 Budapest, Hungary; Institute of Organic Chemistry, HUN-REN Research Centre for Natural Sciences, H-1117 Budapest, Hungary

Laura Bereczki – Centre for Structural Sciences, HUN-REN Research Centre for Natural Sciences, H-1117 Budapest, Hungary; Institute of Materials and Environmental Chemistry, HUN-REN Research Centre for Natural Sciences, H-1117 Budapest, Hungary; [orcid.org/0000-0003-0615-4361](https://orcid.org/0000-0003-0615-4361)

Valerio B. Di Marco – Department of Chemical Sciences, University of Padova, 35131 Padova, Italy; [orcid.org/0000-0001-6108-746X](https://orcid.org/0000-0001-6108-746X)

Petra Bombicz – Centre for Structural Sciences, HUN-REN Research Centre for Natural Sciences, H-1117 Budapest, Hungary; [orcid.org/0000-0002-5509-1515](https://orcid.org/0000-0002-5509-1515)

Complete contact information is available at:

<https://pubs.acs.org/doi/10.1021/acs.cgd.3c01118>

### Funding

Support by the National Research, Development and Innovation Fund NKFI (Hungary) through projects OTKA K-124544 and K-146790 and 2021-4.1.2 NEMZ\_KI-2022-00016 is gratefully acknowledged. N.V.M. acknowledges the financial support from the J. Bolyai Research Scholarship of the Hungarian Academy of Sciences. The authors thank Dr. Christian Schürmann from Rigaku Oxford Diffraction for carrying out a confirmatory measurement for compound B7.

### Notes

The authors declare no competing financial interest.

## ■ REFERENCES

- (1) Dawson, H. M. CXL—Keto-Enolic Tautomerism and the Absorption Spectra of the Aliphatic Ketones. *J. Chem. Soc., Trans.* **1913**, 103 (0), 1308–1316.
- (2) Santos, R. C.; Figueira, R. M. B. M.; Piedade, M. F. M.; Diogo, H. P.; da Piedade, M. E. M. Energetics and Structure of Hydroxynicotinic Acids. Crystal Structures of 2-, 4-, 6-Hydroxynicotinic and 5-Chloro-6-Hydroxynicotinic Acids. *J. Phys. Chem. B* **2009**, *113* (43), 14291–14309.
- (3) Long, S.; Zhang, M.; Zhou, P.; Yu, F.; Parkin, S.; Li, T. Tautomeric Polymorphism of 4-Hydroxynicotinic Acid. *Cryst. Growth Des.* **2016**, *16* (5), 2573–2580.
- (4) Crisponi, G.; Dean, A.; Di Marco, V.; Lachowicz, J. I.; Nurchi, V. M.; Remelli, M.; Tapparo, A. Different Approaches to the Study of Chelating Agents for Iron and Aluminium Overload Pathologies. *Anal. Bioanal. Chem.* **2013**, *405* (2–3), 585–601.
- (5) Dean, A.; Ferlin, M. G.; Carta, D.; Jakusch, T.; Kiss, T.; Faccioli, F. F.; Parrasia, S.; Marton, D.; Venzo, A.; Di Marco, V. B. 4-Hydroxy-3,5-Pyridinedicarboxylic Acids: Synthesis, Complexation Properties Towards Fe(III), Al(III), Cu(II), Zn(II), Human Serum Albumin, and Cellular Toxicity. *J. Solution Chem.* **2018**, *47* (1), 92–106.
- (6) May, N. V.; Gál, G. T.; Szentendrei, Z.; Korecz, L.; May, Z.; Ferlin, M. G.; Dean, A.; Bombicz, P.; Di Marco, V. B. Relationship between Solid State Structure and Solution Stability of Copper(II)-Hydroxypyridinecarboxylate Complexes. *New J. Chem.* **2019**, *43* (27), 10699–10710.
- (7) May, N. V.; Nys, K.; Ching, H. Y. V.; Bereczki, L.; Holczbauer, T.; Di Marco, V. B.; Bombicz, P. Crystal Structures of Zinc(II) Complexes with  $\beta$ -Hydroxypyridinecarboxylate Ligands: Examples of Structure-Directing Effects Used in Inorganic Crystal Engineering. *Acta Crystallogr. B Struct. Sci. Cryst. Eng. Mater.* **2021**, *77* (2), 193–204.
- (8) Di Marco, V. B.; Dean, A.; Ferlin, M. G.; Yokel, R. A.; Li, H.; Venzo, A.; Bombi, G. G. Methyl-Hydroxypyridinecarboxylic Acids as Possible Bidentate Chelating Agents for Aluminium (<sc> > III</sc>): Synthesis and Metal–Ligand Solution Chemistry. *Eur. J. Inorg. Chem.* **2006**, *2006* (6), 1284–1293.
- (9) Dean, A.; Ferlin, M. G.; Brun, P.; Castagliuolo, I.; Yokel, R. A.; Badocco, D.; Pastore, P.; Venzo, A.; Bombi, G. G.; Di Marco, V. B. 1,6-Dimethyl-4-Hydroxy-3-Pyridinecarboxylic Acid and 4-Hydroxy-2-Methyl-3-Pyridinecarboxylic Acid as New Possible Chelating Agents for Iron and Aluminium. *Dalton Trans.* **2009**, No. 10, 1815–1824.
- (10) Dean, A.; Sija, É.; Zsigó, É.; Ferlin, M. G.; Marton, D.; Gandin, V.; Marzano, C.; Badocco, D.; Pastore, P.; Venzo, A.; Bertani, R.; Kiss, T.; Di Marco, V. Possible Chelating Agents for Iron and Aluminium – 4-Hydroxy-5-methyl- and 4-Hydroxy-1,5-dimethyl-3-pyridinecarboxylic Acid. *Eur. J. Inorg. Chem.* **2013**, *2013* (8), 1310–1319.
- (11) Higashi, T. NUMABS, Rev. 2002; Rigaku/MSI Inc.: The Woodlands, TX, 1998.
- (12) CrystalClear; Rigaku/MSI Inc., 2008.
- (13) Burla, M. C.; Caliendo, R.; Carrozzini, B.; Cascarano, G. L.; Cuocci, C.; Giacovazzo, C.; Mallamo, M.; Mazzzone, A.; Polidori, G. Crystal Structure Determination and Refinement via SIR2014. *J. Appl. Crystallogr.* **2015**, *48* (1), 306–309.
- (14) SHELXL-2013, Program for Crystal Structure Solution; University of Göttingen: Germany, 2013.
- (15) Sheldrick, G. M. A Short History of SHELX. *Acta Crystallogr., Sect. A: Found. Crystallogr.* **2008**, *64* (1), 112–122.
- (16) Farrugia, L. J. WinGX and ORTEP for Windows: An Update. *J. Appl. Crystallogr.* **2012**, *45* (4), 849–854.
- (17) Spek, A. L. Structure Validation in Chemical Crystallography. *Acta Crystallogr., Sect. D: Biol. Crystallogr.* **2009**, *65* (2), 148–155.
- (18) Spek, A. L. Single-Crystal Structure Validation with the Program PLATON. *J. Appl. Crystallogr.* **2003**, *36* (1), 7–13.
- (19) Macrae, C. F.; Edgington, P. R.; McCabe, P.; Pidcock, E.; Shields, G. P.; Taylor, R.; Towler, M.; van de Streek, J. Mercury: Visualization and Analysis of Crystal Structures. *J. Appl. Crystallogr.* **2006**, *39* (3), 453–457.
- (20) Allen, F. H.; Johnson, O.; Shields, G. P.; Smith, B. R.; Towler, M. CIF Applications. XV. *EnCIFer*: A Program for Viewing, Editing and Visualizing CIFs. *J. Appl. Crystallogr.* **2004**, *37* (2), 335–338.
- (21) Spackman, M. A.; Jayatilaka, D. Hirshfeld Surface Analysis. *CrystEngComm* **2009**, *11* (1), 19–32.



- (22) Spackman, M. A.; McKinnon, J. J. Fingerprinting Intermolecular Interactions in Molecular Crystals. *CrystEngComm* **2002**, *4* (66), 378–392.
- (23) McKinnon, J. J.; Spackman, M. A.; Mitchell, A. S. Novel Tools for Visualizing and Exploring Intermolecular Interactions in Molecular Crystals. *Acta Crystallogr., Sect. B: Struct. Sci.* **2004**, *60* (6), 627–668.
- (24) McKinnon, J. J.; Jayatilaka, D.; Spackman, M. A. Towards Quantitative Analysis of Intermolecular Interactions with Hirshfeld Surfaces. *Chem. Commun.* **2007**, 3814–3816.
- (25) Bird, C. W. A New Aromaticity Index and Its Application to Five-Membered Ring Heterocycles. *Tetrahedron* **1985**, *41* (7), 1409–1414.
- (26) Gordy, W. Dependence of Bond Order and of Bond Energy Upon Bond Length. *J. Chem. Phys.* **1947**, *15* (5), 305–310.
- (27) Kotelevskii, S. I.; Prezhdo, O. V. Aromaticity Indices Revisited: Refinement and Application to Certain Five-Membered Ring Heterocycles. *Tetrahedron* **2001**, *57* (27), 5715–5729.
- (28) Di Marco, V. B.; Yokel, R. A.; Ferlin, M. G.; Tapparo, A.; Bombi, G. G. Evaluation of 3,4-Hydroxypyridinecarboxylic Acids as Possible Bidentate Chelating Agents for Aluminium(III): Synthesis and Metal–Ligand Solution Chemistry. *Eur. J. Inorg. Chem.* **2002**, 2002 (10), 2648–2655.
- (29) Dean, A. Sintesi e Studio Delle Interazioni Metallo—Legante per Nuove Molecole Potenzialmente Impiegabili Nella Terapia di Chelazione di Ferro(III) e Alluminio(III), PhD Thesis; University of Padova: Padova, 2008.
- (30) Dean, A.; Ferlin, M. G.; Brun, P.; Castagliuolo, I.; Yokel, R. A.; Venzo, A.; Bombi, G. G.; Di Marco, V. B. Evaluation of 4-Hydroxy-6-Methyl-3-Pyridinecarboxylic Acid and 2,6-Dimethyl-4-Hydroxy-3-Pyridinecarboxylic Acid as Chelating Agents for Iron and Aluminium. *Inorg. Chim. Acta* **2011**, *373* (1), 179–186.
- (31) Dean, A.; Ferlin, M. G.; Carta, D.; Jakusch, T.; Kiss, T.; Faccioli, F. F.; Parrasia, S.; Marton, D.; Venzo, A.; Di Marco, V. B. 4-Hydroxy-3,5-Pyridinedicarboxylic Acids: Synthesis, Complexation Properties Towards Fe(III), Al(III), Cu(II), Zn(II), Human Serum Albumin, and Cellular Toxicity. *J. Solution Chem.* **2018**, *47* (1), 92–106.
- (32) Katritzky, A. R.; Lagowski, J. M. *The Principles of Heterocyclic Chemistry*; Academic Press: New York, 1968.
- (33) Resnati, G.; Boldyreva, E.; Bombicz, P.; Kawano, M. Supramolecular Interactions in the Solid State. *IUCrJ* **2015**, *2* (6), 675–690.
- (34) Bombicz, P.; Gruber, T.; Fischer, C.; Weber, E.; Kálmán, A. Fine Tuning of Crystal Architecture by Intermolecular Interactions: Synthon Engineering. *CrystEngComm* **2014**, *16* (18), 3646–3654.
- (35) Grell, J.; Bernstein, J.; Tinhofer, G. Graph-Set Analysis of Hydrogen-Bond Patterns: Some Mathematical Concepts. *Acta Crystallogr., Sect. B: Struct. Sci.* **1999**, *55* (6), 1030–1043.